AGU PUBLICATIONS

Water Resources Research

RESEARCH ARTICLE

10.1002/2013WR015006

Scaling properties of tidal networks

Mirian Jiménez[1], Sonia Castanedo[1], Zeng Zhou[1], Giovanni Coco[1], Raúl Medina[1], and Ignacio Rodriguez-Iturbe[2]

[1]Environmental Hydraulics Institute "IH Cantabria," Universidad de Cantabria, Santander, Spain, [2]Department of Civil and Environmental Engineering, Princeton University, Princeton, New Jersey, USA

Key Points:
- Tidal network structure derived from estuarine hydrodynamics
- Tidal networks evolve toward a minimum energy expenditure state
- Scale behavior is found in accumulated drainage area and volume

Correspondence to:
M. Jiménez,
mirian.jimenez@unican.es

Citation:
Jiménez, M., S. Castanedo, Z. Zhou, G. Coco, R. Medina, and I. Rodriguez-Iturbe (2014), Scaling properties of tidal networks, *Water Resour. Res.*, *50*, 4585–4602, doi:10.1002/2013WR015006.

Received 7 NOV 2013
Accepted 19 MAY 2014
Accepted article online 26 MAY 2014
Published online 4 JUN 2014

Abstract A new methodology is developed to extract tidal network from hydrodynamic conditions, and use data derived from numerical modeling or field observations to test the hypothesis that tidal networks are characterized by scale-invariant properties. Different tidal network configurations have been obtained from long-term numerical simulations in an idealized basin. These simulations show the influence of hydrodynamic conditions (tidal range, *TR*) and sediment (grain size sediment, D_{50}) on the final configuration of the network. One of the signatures of scale-invariant behavior is related to the presence of a power law relationship in the probability distribution of geometrical characteristics. For each model configuration and field site, the probability distribution of drainage area and the drainage volume has been calculated, and in both cases tidal networks show scale-invariant characteristics. After assessing the sensitivity of the results, an energy expenditure analysis shows that tidal basins evolve toward a state with less morphodynamic activity, with a lower energy expenditure compare with the initial state.

1. Introduction

Tidal basins sustain rich ecosystems, providing food and habitat necessary for the survival of various species as well as many socioeconomic services and activities [*Costanza et al*., 1989]. Understanding the morphological evolution of tidal basins would allow to properly assess the changes induced by fluctuations in natural and anthropogenic drives. To achieve this objective, we need to deepen existing knowledge of the mechanisms that keep these systems in the so-called dynamic equilibrium (where sediment fluxes balance each other over a certain time scale).

The structure of the channel network depends on the external drivers. *van Maanen et al*. [2013a] studied the effects of variations in the tidal range and the depth of the initially unchannelized tidal basin on the evolution of the morphology of the system. They show that a higher tidal range and/or a smaller basin depth induce the formation of tidal networks more rapidly. The influence of sea level rise and the related morphodynamics have been studied over the last decades. *Friedrichs et al*. [1990] investigated the impact of SLR on several tidal basins in the United States and found that the sediment import or export depends on the geometrics characteristics of each system (e.g., constant bank slope or curved bank slope). *Van Goor et al*. [2003] used an aggregated scale model ASMITA to simulate the long-term morphological response of a tidal inlet to rising sea levels. *Dissanayake et al*. [2012] studied the impacts of different scenarios of sea level rise (SLR) in the Ameland inlet using a process-based model. All these studies showed us that these systems are vulnerable to sea level fluctuations, decreasing intertidal areas and sometime even shifting the whole system from sediment-exporting (ebb-dominated) to sediment-importing (flood-dominated) [*Van der Wegen*, 2013]. *van Maanen et al*. [2013b] simulated the evolution of a short tidal basin in response to a rising sea level and also concluded that SLR produces changes in the location and number of channels in the basin, and even tidal asymmetry.

It is thus of utmost importance to understand how the network structure is linked to external dynamic factors and to properly forecast new equilibrium states and characteristics when changes in the drivers are induced.

In the last decades, advances in Digital Elevation Models (DEMs) acquisition and analysis have lead to an increasing interest in the problem for network extraction for natural systems and the study of network behavior [e.g., *Montgomery and Dietrich*, 1988; *Passalacqua et al*., 2010]. Network extraction in the case of estuaries is a complicated problem, mainly because the drainage direction is time dependent. *Fagherazzi*

et al. [1999] proposed a methodology to extract the tidal network of estuaries by means of a multicriteria algorithm (elevation threshold and curvature threshold criteria). However, in the case of estuaries, at least conceptually, it is not the bed topography but the free surface flow gradients that drive hydrodynamics and sedimentary processes.

From a modeling perspective, *Rinaldo et al*. [1999a] simplified the 2-D momentum equations for shallow water using the Poisson assumption which implies that the propagation of the tidal wave in the channels is instantaneous, and drainage directions can be resolved by evaluating water surface gradients. They also analyzed the scaling relationships of tidal landforms comparing them with analogous ones found in fluvial systems [*Rodriguez-Iturbe and Rinaldo*, 1997]. One of the signatures of scale-invariant behavior is related to the presence of power law relationships in the probability distribution of geometrical characteristics. *Rinaldo et al*. [1999a] analyzed the exceedance probability of watershed area, total length, width of the tidal channel cross section and botanical mass. Presence of power law behavior would imply that these relationships are straight lines in double logarithmic plots over an extended range of scales. Contrary to the case of river networks, the features analyzed for tidal networks did not present well-defined power law relationships, showing no scale-invariant properties. *Rinaldo et al*. [1999b, 1999c] found power law relationships of cross-sectional channel area, drainage area, and tidal prism when related to peak discharge during spring tides. However, these power laws were present only for channels with cross-sectional areas greater than about 50 m^2. These restrictions were attributed to an inadequate spatial resolution of the DEM and to the assumptions in the hydrodynamic model. *Fagherazzi and Furbish* [2001] suggested that power law scaling could break due to specific characteristics of the tidal basin under analysis. In particular, they studied the Venice lagoon and argued that different resistance to erosion in different layers and regions of the lagoon may have broken the power law behavior.

The drainage network in a river basin display tree-like structures, with a unidirectional flux that provides efficient means of transportation for runoff and sediment. In tidal systems, the interaction of ebb and flood flows induces the existence of loopy drainage networks due to the bidirectionality of the flux, so that flow pathways can radically change between flood and ebb. To overcome this problem, different authors have recently developed graph theoretic analyses for loopy networks [*Katifori and Magnasco*, 2012; *Mileyko et al*., 2012]. Specifically, they assign a weight function to the loop edges so that the reticular/loopy network can be turned into a loopless tree-like network. The results, tools, and methodologies presented in these studies are useful to obtain loopless and unidirectional networks starting from tidal hydrodynamic conditions.

Power law relationships represent long-term characteristics of the system but do not address how these configurations are reached. On the other hand, several developments in the numerical modeling of the hydrodynamics and morphodynamics of natural systems have been accomplished over the last decade allowing to simulate tidal network morphodynamics from incipient channel formation to long-term equilibrium. Different 2-D numerical models have been used to describe the morphogenesis and development of tidal networks [*Marciano et al*., 2005; *D'Alpaos*, 2005; *Di Silvio et al*., 2010; *van Maanen et al*., 2013a, 2013b]. While most of these authors have focused on simulating the development of tidal networks and the physical mechanism that drive their evolution, only *Marciano et al*. [2005] analyzed the pattern of channel branching in a tidal basin. They showed that smaller channels, and channels that are close to each other, are typical for sites with relative larger overall slopes and with small water depths. The branching behavior obtained in the simulated networks shows similar patterns to those observed in the Wadden Sea.

The geometry and possible fractal nature of tidal channel systems have been widely studied in tidal channel networks around the world [*Cleveringa and Oost*, 1999; *Angeles et al*., 2004; *Novakowski et al*., 2004; *Feola et al*., 2005]. Horton's hierarchical and fractal analyses have been performed in the Wadden Sea by *Cleveringa and Oost* [1999]. They showed that these tidal channel systems have same statistical-self similar fractal characteristics. *Angeles et al*. [2004] determined the fractal dimension using two methods (box counting and contiguity) in nine tidal channels in Bahía Blanca (Argentina). All channels presented similar fractal dimensions (greater than one and lower than two), characteristic of their self-affine fractal features. On the other hand, *Novakowski et al*. [2004] performed a Horton's and Hack' law type of analyses of tidal creeks networks in North Carolina using high-resolution digital images. They reported power law relationships between the maximum channel length and area. *Feola et al*. [2005] studied, by means of a hydrodynamic approach (Poisson model), the probabilities of exceedance of upstream length and unchanneled length in two salt marshes in the Venice lagoon and performed an analysis of the scaling of Hack's law. They showed

that in the tidal case there is no evidence of power laws, thereby suggesting that scale-free behavior is not present.

Several authors have suggested that patterns in nature may be associated with optimal characteristics in terms of energy or entropy. *Rodríguez-Iturbe et al*. [1992b] shows that drainage networks at equilibrium tend to a configuration with minimum energy dissipation. For tidal systems, *Townend and Dun* [2000] focused instead on long-term morphodynamic behavior of an estuarine environment, considering the criterion of constant entropy production rate per unit discharge to define equilibrium conditions. They suggest that when the estuary reaches equilibrium conditions, the longitudinal distribution of total energy through a tidal cycle along an estuary may be represented as exponential function, i.e., the energy at a given section may be expressed by an exponential of a linear function of the distance from the section to the estuary mouth. This statement implies that energy transferred due to the tidal wave will decay exponentially in the upstream direction. Still in the field of tidal system research, *Van Der Wegen et al*. [2008] evaluated the long-term evolution of a tidal embayment in terms of energy dissipation using a 2-D numerical model, demonstrating that energy dissipation decreases over time, and showing that the basins evolve toward a state of less morphodynamic activity (decreasing deepening and widening of the basin, accompanied with stable patterns). This general approach and specifically focus on linking principles of minimum energy dissipation with scale-invariant properties of the network and morphological evolution.

The studies above reveal a lack of consensus on the role of processes leading to long-term equilibrium of intertidal geomorphic features in tidal basins. Thus, the main objective of this paper is to investigate possible relationships between hydrodynamic and topographical characteristics in tidal networks and to search for scale-invariant properties. To achieve this goal, several numerical simulations have been performed in order to obtain different configurations of tidal network depending on the hydrodynamic and sediment conditions. A novel methodology has been developed in order to obtain the drainage network of the system. Moreover, different characteristics have been analyzed looking for scale-invariant properties. Unlike other studies, which extract the tidal network from the bathymetric characteristics [*Fagherazzi et al*., 1999; *Passalacqua et al*., 2010], we analyze the exceedance probability of the drainage area and volume of the tidal network during the ebb and flood time. The analysis is also performed for a real estuary (Santoña's estuary, Spain). In addition, we analyze the possibility that, similar to other natural systems, the emergence of channel networks is a process converging toward minimum energy expenditure. The remainder of this paper is structured as follows: section 2 describes the methodology developed for the extraction of tidal networks and section 3 shows the results of applying the methodology to simplified tidal systems and to a real estuary. Sections 4 and 5 present the discussion of the results and conclusions of the analyses.

2. Methodology

2.1. Numerical Model Description

The numerical model, DELFT3D is used to simulate the time evolution of a channel network in a geometrically simplified configuration similar to the one used by *Marciano et al*. [2005] and *van Maanen et al*. [2013a, 2013b]. DELFT3D is a finite difference numerical model composed of a number of modules: currents, sediment transport, and bottom changes. In this study, we use the 2DH version of the DELFT3D model, which solves the momentum and continuity equations on a grid with a robust wet and dry scheme. A full description of the model can be found in *Lesser et al*. [2004]. It should be pointed out that in the future the role that wind waves, overtides, cohesive material, and vegetation play in the development of tidal networks will be considered.

Sediment transport is calculated using the *Engelund and Hansen* [1967] formulation, where the sediment transport rates are calculated as total load (S) according to

$$S = \frac{0.05U^5}{\sqrt{g}C^3\Delta^2 D_{50}} \tag{1}$$

where S is the sediment transport, U is the magnitude of depth-averaged flow velocity (m/s), Δ is the relative density $(\rho_s - \rho_w)/\rho_w$ (dimensionless) (ρ_s and ρ_w being the sediment and water density, respectively (kg/m^3)), C is the friction parameter defined by $\sqrt[6]{h}/n$ (m$^{1/2}$/s), and D_{50} is the median grain size (m).

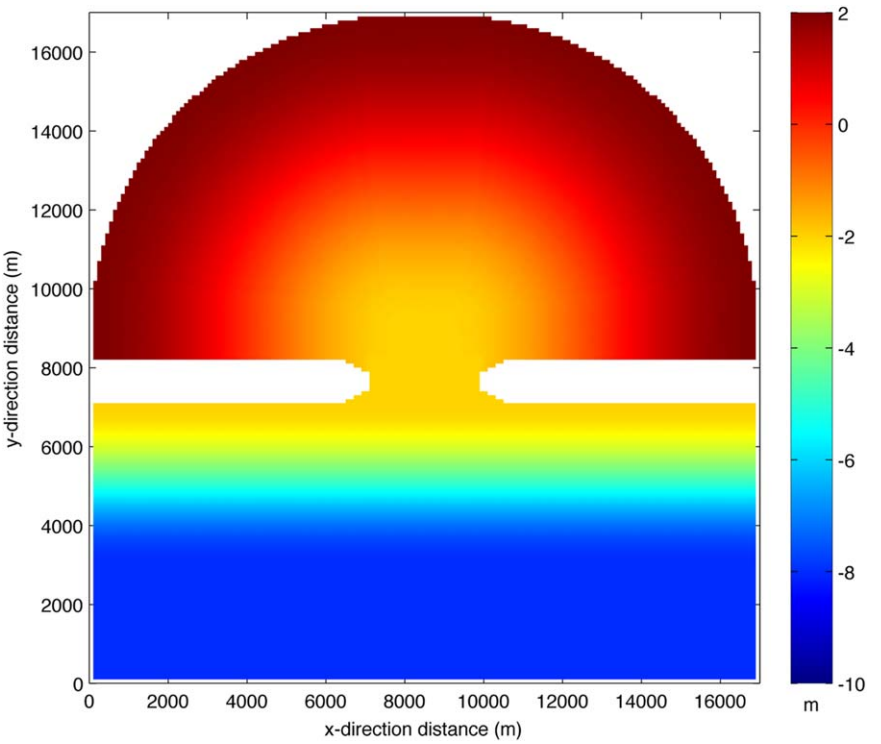

Figure 1. Initial bathymetry for the model simulation.

2.1.1. Model Setup

Hydrodynamic and morphodynamic behavior are solved numerically for a rectangular region of 17 × 17 km^2. Within this region, two different zones are delimited by impermeable and nonerodible barrier islands. An outer, deeper zone representing the open sea and an inner zone, where the tidal network will develop. A regular grid with 100 × 100 m^2 cells is used to solve both the hydrodynamics and the morphodynamics of the system (see Figure 1).

Numerical simulations have been conducted using different sinusoidal tidal ranges as the hydrodynamic forcing (1, 2, and 3 m) and different grain size characteristics (D_{50} = 120, 480, and 960 μm). The model simulations cover a time span of 4000 years. This time period has been selected because of the reduced rates of morphological evolution.

Random perturbations of ±1.5 cm were added to the bed level in the basin to trigger channel pattern development. The position of the initial random perturbations can certainly determine the initialization of the channels and for some channels also their long-term position. Some recent work [*Zhou et al*., 2014a, 2014b] has shown that even though the landscape details are different, some geometric properties like hypsometry can in fact be the same.

Hydrodynamic changes occur on short time scales, while morphological changes occur during much longer time scales. For this reason, when dealing with long-term simulations, *Lesser et al*. [2004] and *Roelvink* [2006] recommend numerically accelerating the evolution by a constant morphological factor. A sensitivity analysis about the morphological factor has been done, determining that a value of 200 is appropriate value for the model presented in this study. Other authors have also used this value for the morphological factor and obtained similar patterns to those observed in nature [*Van der Wegen*, 2013].

2.2. Extraction of Channels Networks

We propose a new method for the extraction of channel networks that takes into account a more accurate hydrodynamic description of the system than the one used in previous studies where a simplified Poisson hydrodynamic model was used [*Rinaldo et al*., 1999a; *Marani et al*., 2003; *D'Alpaos et al*., 2007]. The procedure to identify the channel network involves five steps:

1. The first is the analysis of the drainage directions in the basin. This is determined using a variation of the D8 method (based on eight-neighbor-connectivity) developed by *O'Callaghan and Mark* [1984] and widely used afterward in studies dealing with watershed delineation [*Morris and Heerdegen*, 1988; *Tarboton et al*., 1991; *Tarboton*, 1997]. In the original method, the drainage direction is assigned to each grid cell corresponding to the steepest bed slope. In this study, the drainage direction is the same as the flow direction in each grid cell obtained from the hydrodynamic model (discretization implies that the flow is characterized by only one of eight possible directions separated by an angle of 45°). The complicated hydrodynamics of a tidal system induces continuous changes in drainage directions. For this reason, the drainage directions have been calculated at each time step during both the ebb and flood phases.

The drainage direction in each cell defines the cell to which it is connected, i.e., the cell which receives all the water that flows through the original one. That is to say, each cell can "receive" water from and/or "provide" water to one of its neighbors. In this way, the connectivity can be established for each cell.

2. The second step is to unequivocally define the connectivity between cells. An adjacency matrix, W_{ij}, establishes these relationships between cells. W_{ij} is a representation of a directed graph with a dimension of $(n \times n)$ (n being the number of cells in the grid). The rows represent the index of a possible providing cell, while the columns represent the index of a possible receiving cell. When cell i donates water to cell j, the element of the matrix $W_{i,j}$ is set to one, and when no link exists, W_{ij} is set to zero.

As previously mentioned, the presence of loops in the channel network leads to inconsistencies in the algorithm for the drainage area computation. To avoid this problem, *Katifori and Magnasco* [2012] and *Mileyko et al*. [2012] carried out a hierarchical decomposition of loopy networks into tree-like networks based on the channel widths.

This hierarchical decomposition assumes that loops can be unrolled starting with the loop containing the narrowest link. That is, during first step, all the loops are detected. The narrowest link belonging to a loop is then removed, setting to zero its corresponding coefficient in the adjacency matrix. This operation will break at least one loop but may break more. Thus, once the narrowest link is removed, the loop detecting algorithm is used again to determine which loops still exists. If there are still loops to unroll we proceed again looking for the narrowest link of the links belonging to a loop. That link is removed again and the procedure repeated until no more loops exist. At this point, the original network has been transformed into a directed tree. In our study, all cells that belong to a loop are detected, and the existing link between the first cell detected in the loops and the last cell involved is set to zero in the adjacency matrix.

All loops are unrolled in this way until a completely directed tree-like adjacency matrix is achieved. Once the directed adjacency matrix is obtained, the contributing area in each grid cell can be calculated.

3. The basic algorithm that computes the total drainage area to each grid cell, A_i, is a recursive algorithm based on *Rodriguez-Iturbe and Rinaldo* [1997].

$$A_i^k = \sum_j W_{ij}^k A_j^k + a_i \tag{2}$$

where A_i denotes the total drainage area at time k, i.e., the number of pixels draining through cell i, a_i is the inner area of cell, i, the subindex j spans the eight neighboring cells, and $W_{i,j}$ is a functional operator that determines the eventual presence of a connection:

$$W_{ij}^k = \begin{cases} 1 & \text{if } i,j \text{ are connected} \\ 0 & \text{otherwise} \end{cases} \tag{3}$$

4. In tidal systems, at each time step, an increase or decrease of water level is accompanied by a change in flow velocities. Therefore, the total drainage volume in each cell, V_i can be computed as

$$V_i^k = \sum_{k=0}^{k=m} W_{ij}^k V_j^k + v_i \tag{4}$$

with

$$v_i = a_i . \Delta\eta_i \tag{5}$$

where V_i denotes the total drainage volume in a tidal phase through the cell i; m is the number of time steps for the tidal phase; v_i is the drainage volume of cell i; a_i is the inner area of cell i, and $\Delta\eta_i$ is the variation of the water surface between two consecutive time steps in the cell i.

$$\Delta\eta_i = \begin{cases} (\eta_i(k) - \eta_i(k+1)) & \text{for ebb tide} \\ (\eta_i(k+1) - \eta_i(k)) & \text{for flood tide} \end{cases} \tag{6}$$

The subindex j spans the eight neighboring cells and $W_{i,j}$ is a functional operator that determines the eventual presence of a connection. Drainage area and drainage volume are computed for each time step, t, during the ebbing or flooding phase. Therefore, the tidal prism, Ω, is defined as the total water volume exchanged through the outlet between low tide and high tide:

$$\Omega = \sum_{k=0}^{k=m} \sum_{i=1}^{i=n} V_i . dk \tag{7}$$

where n is the number of pixels which are localized in the outlet and m is the number of time steps used to discretize an ebbing or flooding phase.

5. Finally, the channel network is defined by the cells that exceed a drainage volume threshold (above this threshold, the flow is considered to be totally channeled). The objective determination of this threshold is still an open issue and distinguishes between channels and flats. In this study, the threshold has been defined by the x_{min} parameter, x_{min} is a parameter representing the point over which scale invariant is observed. It marks a regime change in the estuarine dynamics, where the overall aggregation behavior that characterizes scale invariance becomes dominant. It is obtained from the power law fitting (section 2.3).

2.3. Scale-Invariant Relationships

In order to search for scale-invariant relationships, such as those found in river networks [*Rodriguez-Iturbe and Rinaldo*, 1997], we calculate the exceedance probability distributions of drainage area and volume. The power law exponent is estimated using a linear regression to log-transformed values in the exceedance probability distribution. We used the approach developed by *Clauset et al*. [2009] to estimate the exponents of the power law (maximum-likelihood estimate, MLE, methods are combined with goodness-of-fit tests based on the Kolmogorov-Smirnov statistic, K-S). This approach provides the scaling parameter β and the lower limit, x_{min}, of the scale region, over which the power law behavior is valid. MLE determines the parameter values that maximize the likelihood of the model given the observed data and it has been shown to be the single best approach for estimating the power law exponent (β) [*Newman*, 2005; *White et al*., 2008]. In this study, the lower bound for the fitting is provided by the x_{min} parameter, over which power law behavior can be observed. This value is quantified from a K-S test, which uses the maximum distance, D, between the probability distribution of the data and the fitted model:

$$D = \max_{x \geq xmin} |S(x) - P(x)| \tag{8}$$

where $S(x)$ is the probability distribution of the data with value at least x_{min} and $P(x)$ is the probability distribution for the power law model that best fits the data in the region $x \geq x_{min}$; x_{min} is selected to minimize D. Physically, it corresponds to a minimum basin size under which channels obtained in this work do not develop.

The upper bound is defined by "finite size effects," which can be seen as a deviation from power law behavior at large values of drainage volume in the exceedance probability plot. Finite size effects appear when only a small number of pixels are associated with very larger values of areas and volumes, causing a loss of statistical significance.

2.4. Minimum Energy Expenditure

Optimization criteria, such as minimum energy expenditure, are often used to explain spatial and topological patterns in natural systems [*Stevens*, 1974].

In river basins, whose optimal channel network structure (OCN) can be explained in terms of the optimization of energy expenditure [*Rodriguez-Iturbe and Rinaldo*, 1997]. The optimization of energy expenditure in OCNs involves the combination of shear stress and sediment transport criteria in order to describe energy dissipation. In tidal systems, bed friction is the most important mechanism in terms of energy dissipation. It arises as a resistance force between the moving flow and the fixed bottom. Besides bed friction, the shape of the channels plays an important role on tidal propagation [*Friedrichs and Aubrey*, 1994; *Lanzoni and Seminara*, 1998].

In our study, the energy expenditure of the system has been computed at different stages of the morphodynamic evolution of the basin. The analysis has been carried out for different configurations of the two of parameters controlling the basin evolution: tidal amplitude and sediment grain size. For any given stage of the evolution, and any given point in the tidal basin, energy expenditure, E_i, is computed as the integral of the dissipated power in a tidal cycle. Dissipated power is the product of the bed shear force, F (the stress $\times$ area), and the velocity of the flow:

$$E_i(t) = \int_{t=0}^{t=m} \vec{F}.\vec{U}.dt \tag{9}$$

$$\vec{F} = \zeta.a_i \tag{10}$$

where ζ is the bed shear stress (N/m^2), a_i is the cell area (m^2), and $\vec{U}$ is the velocity (m/s). The energy dissipation of the basin is the sum of the energy dissipation of all cells.

3. Results

3.1. Numerical Simulations

Numerical simulations given in Figure 2 show the development of tidal networks after 4000 years for different combinations of tidal range and grain sizes. As can be observed that the higher the tidal range, the greater the area affected in the tidal basin, and the bigger the number of channels that are formed in the inner basin. Also the influence of grain size can be detected in the tidal network structure. When smaller sediment sizes are present (Figures 2a, 2d, and 2g), a greater amount of sediment is mobilized, leading to more complex morphologies and faster morphodynamic evolution.

3.2. Network Extraction

The methodology described in section 2.2 has been applied to each simulation presented in Figure 2. Different steps of the methodology are depicted in Figure 3. Figure 3a illustrates the topography obtained with a tidal range of 2 m and a grain size of 120 μm after 4000 years. For the ebb and flood phases, velocity fields at discrete time intervals have been obtained. In Figure 3b, an example of the velocity field during the ebb phase is showed. The direction of the vectors determines the direction of the flux, and the color represents the magnitude of the velocity. The drainage direction for each pixel was assigned based on the direction of the velocity vector to one of eight possible directions, each of them covering 45°. In Figure 3c, we show the values from 1 to 8 (one for every possible direction) assigned following the previous method. Figure 3c helps us to visualize how the flux is distributed in the basin and how it is organized toward the mouth. Figure 3d shows the total volume drained at each cell during an ebb phase. As expected, the tidal channels contain the majority of the flux in the system. This is particularly evident when the water has left the adjacent tidal flat surface and the flux becomes increasingly confined to the channels. The same analysis has been carried out for each of the morphologies shown in Figure 2.

In Figure 4, the channel networks in a falling and rising tide are depicted for morphologies with $D_{50} = 480$ μm and tidal ranges of 1 m (Figures 4a and 4b), 2 m (Figure 4c and 4d), and 3 m (Figures 4d and 4e), respectively. The figures on the left row show the tidal network obtained during a flood phase and those on the right row shows similar to that during the ebb phase. The greater the tidal range, the bigger the volume in the system. During both phases the networks present similar characteristics in the distribution of the main channels, although during ebbs the flow is more concentrated in the main channels.

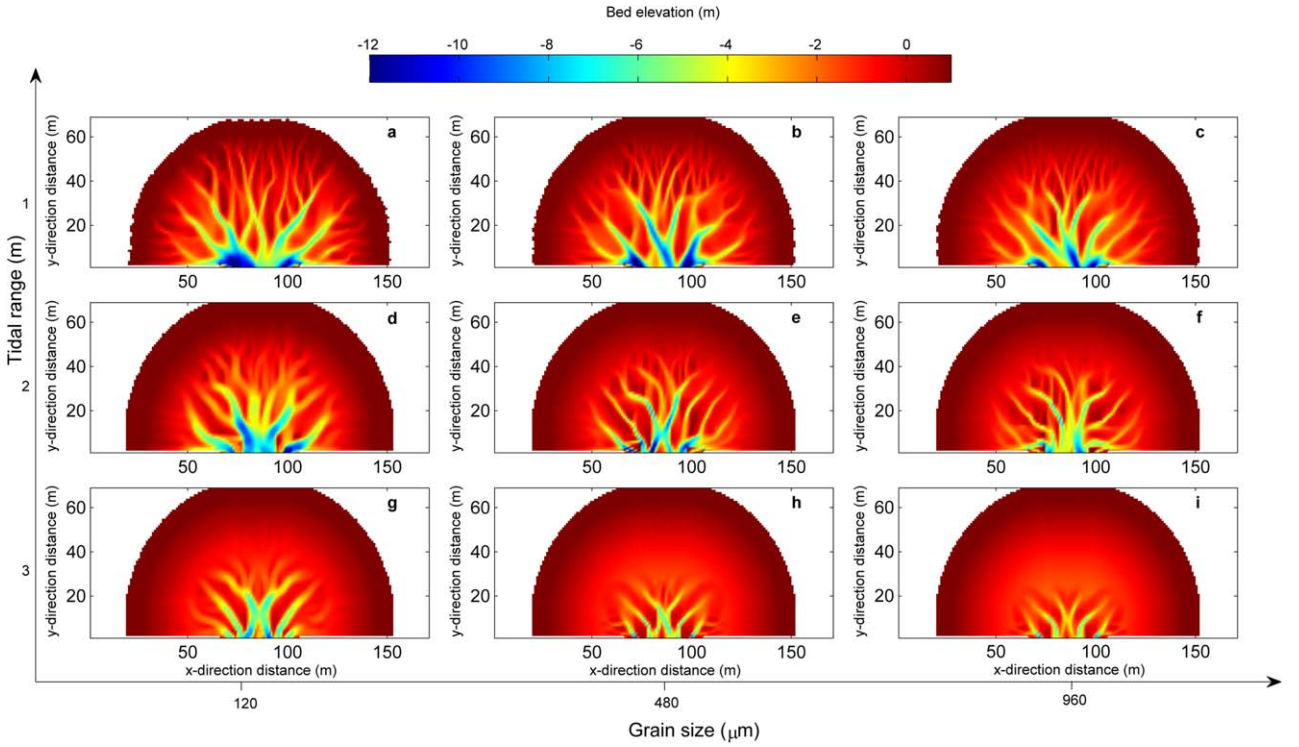

Figure 2. Numerical simulations of tidal network development after 4000 years for different tidal range (*TR*) and grain size (D_{50}). (a) $TR = 3$ m with $D_{50} = 120$ μm, (b) $TR = 3$ m with $D_{50} = 480$ μm, (c) $TR = 3$ m with $D_{50} = 960$ μm, (d) $TR = 2$ m with $D_{50} = 120$ μm, (e) $TR = 2$ m with $D_{50} = 480$ μm, (f) $TR = 2$ m with $D_{50} = 960$ μm, (g) $TR = 1$ m with $D_{50} = 120$ μm, (h) $TR = 1$ m with $D_{50} = 480$ μm, and (i) $TR = 1$ m with $D_{50} = 960$ μm.

3.3. Power Law Fitting

Power laws are signatures of self-similarity phenomena that have the same characteristics across many scales, from small to large scales [*Rodriguez-Iturbe and Rinaldo*, 1997].

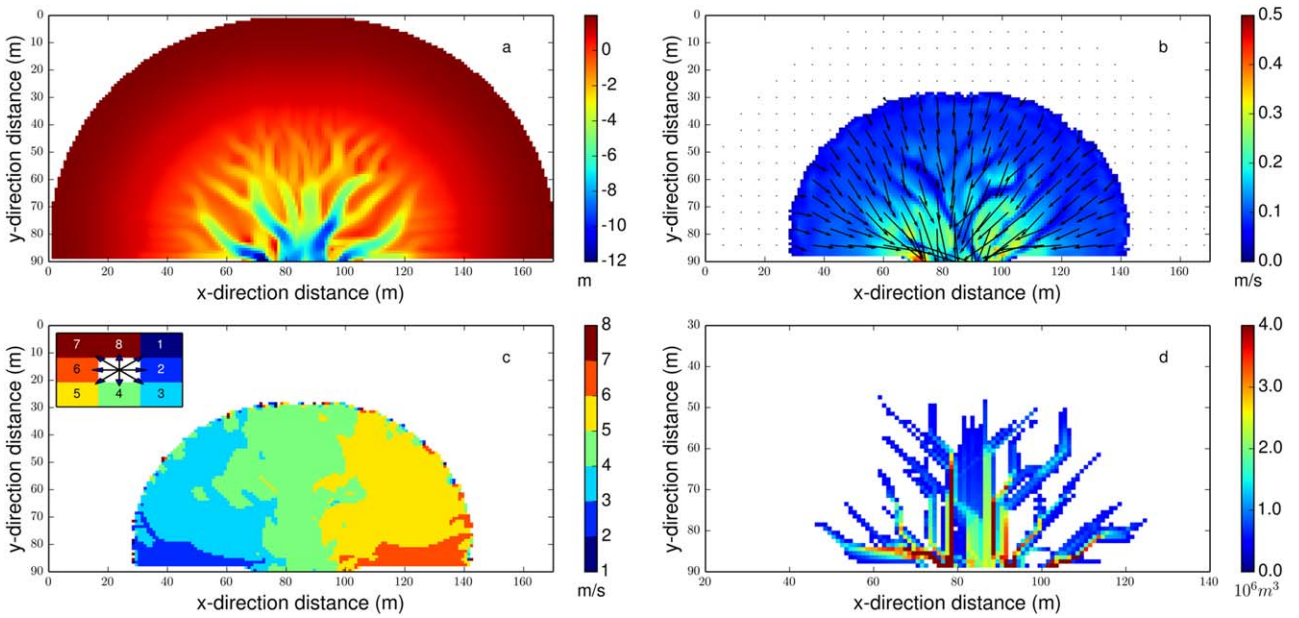

Figure 3. Representation of the different steps of the methodology for the simulation with $TR = 2$ m and $D_{50} = 120$ μm: (a) Morphology obtained after 4000 years (bed elevation (m)), (b) velocity field during ebb tide, (c) drainage directions determined by an eight-connectivity method during a time step in the ebb phase, and (d) drainage volume in each grid cell (m^3) during an ebbing phase.

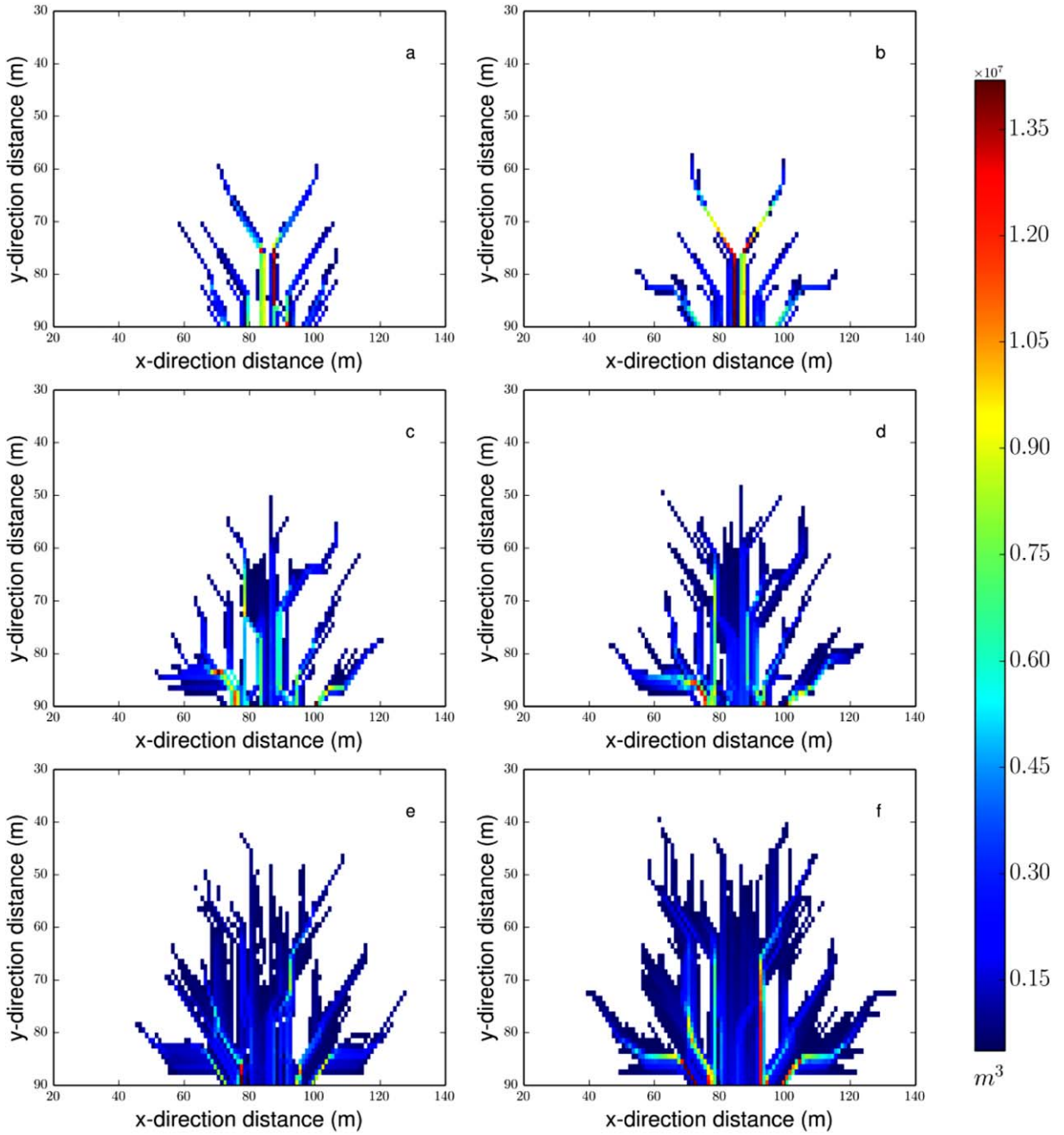

Figure 4. Drainage volume in each grid cell extracted from the morphologies simulated with $D_{50} = 480$ μm and $TR = 1$, 2, and 3 m during (a, c, e) flood and (b, d, f) ebb tide. Each row refers to results for $TR = 1$, 2, and 3 m (from top to bottom).

Rodríguez-Iturbe et al. [1992b] found that the probability distribution of the drainage area in river basins follows a power law of the form $P[A > a] \propto a^{-\beta}$ with $\beta \approx 0.43 \pm 0.02$, a result that is consistent for many basins. Analogously, in this section we investigate the scaling properties of the drainage area and drainage volume numerically simulated in tidal networks during the ebbing and flooding phase.

Figures 5 and 6 show the exceedance probability of the drainage area and drainage volume, respectively, for the flooding and the ebbing phases. A similar slope is detected for different tidal ranges and grain sizes. Power law fits to the probability distribution of drainage area and drainage volume have been carried out separately during flood and ebb.

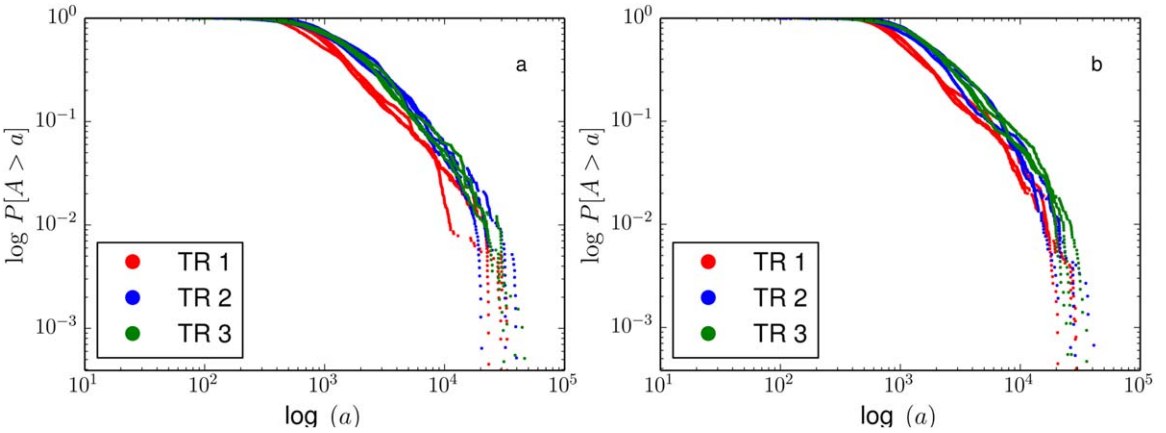

Figure 5. Double logarithmic plot of the exceedance probability of drainage area P ($A \geq a$) at any point of the network (versus the current value of a expressed in m^2) computed for different tidal ranges during (a) flooding phase and (b) ebbing phase.

Figure 7 illustrates in more detail an example of the exceedance probability of drainage area (Figures 7a and 7b) and drainage volume (Figures 7c and 7d) for the morphology with tidal range of 1 m and D_{50} of 120 μm during flood and ebb. This figure shows that the slopes obtained during falling and rising tides remain similar and that the exceedance probability follows straight lines for almost two orders of magnitude. In Table 1, the exponents obtained from the power law fitting β for drainage area for each morphology are presented, while Table 2 shows the exponents obtained from the power law fitting for drainage volume. The drainage area distribution is defined by the relationship $P[A > a] \propto a^{-1.39 \pm 0.14}$ and the drainage volume by $P[V > v] \propto v^{-1.40 \pm 0.13}$.

For this reason, the value of β should be relatively unaffected by the size of the system. Figure 8 shows the distribution of drainage volume for the whole system (gray line) and for a subsystem contained within it (black line). As can be seen, the slope remains practically unchanged, with a $\beta = 1.34$ in the total basin and $\beta = 1.32$ in the "subsystem."

Finally, analyses have been carried out to evaluate the evolution of the probability distribution over the time. Figure 9 displays the evolution of the exceedance probability of drainage volume over time as a tidal basin, with a tidal range of 3 m and grain size of 480 μm, evolves toward equilibrium. As tidal networks developed, the exceedance probability of drainage volume evolves toward a power law distribution with the largest changes occurring in the upper part of the distribution. This is an indication of the formation of small channels and associated intertidal areas which increase small drainage volumes. The overall shift of

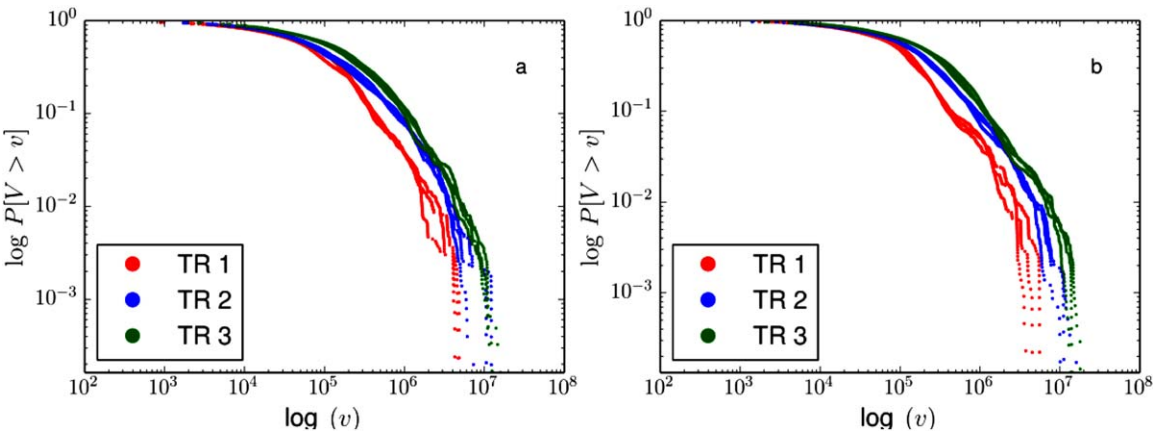

Figure 6. Double logarithmic plot of the exceedance probability of drainage volume P ($V \geq v$) at any point of the network (versus the current value of v expressed in m^3) computed for different tidal ranges during (a) flooding phase and (b) ebbing phase.

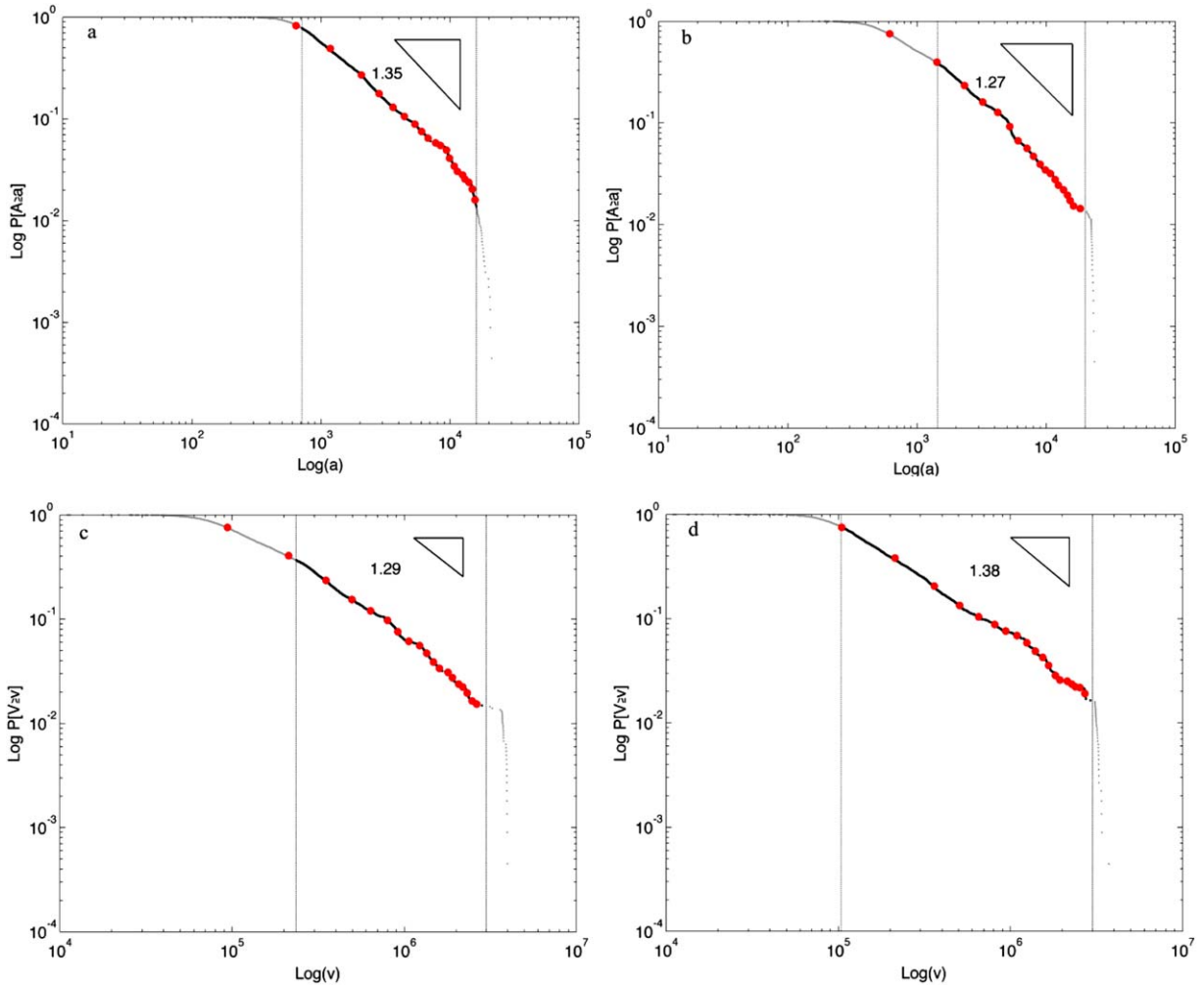

Figure 7. (a and b) Double logarithmic plot of the exceedance probability of drainage area P ($A \geq a$) at any point of the network (versus the current value of a expressed in m^2) computed for the morphology with $TR = 1$ m and $D_{50} = 120$ μm. (a) Flooding phase and (b) ebbing phase. (c and d) Double logarithmic plot of the exceedance probability of drainage volume P ($V \geq v$) (versus the current value of a expressed in m^3) computed for the morphology with $TR = 1$ m and $D_{50} = 120$ μm. (c) Flooding phase and (d) ebbing phase.

the curve indicates an increase in tidal prism concomitant with the development of channel network. Physically, tidal prism increases because the system is ebb-dominated leading to erosion of sediment in the basin (implying larger tidal prism) and the formation of an offshore delta.

Table 1. Values of Coefficient β, Fitting a Power Law to Each Simulated Morphology in the Drainage Area Distribution

			Coefficient (β)		x_{min} (m^2)	
Simulation	Tidal Range (m)	D_{50} (μm)	Flood Tide	Ebb Tide	Flood Tide	Ebb Tide
Morphology 1	1	120	1.27	1.34	1457	714
Morphology 2	1	480	1.34	1.36	1152	1473
Morphology 3	1	960	1.4	1.41	1158	937
Morphology 4	2	120	1.26	1.37	4326	2105
Morphology 5	2	480	1.33	1.55	1396	1363
Morphology 6	2	960	1.34	1.32	2433	1628
Morphology 7	3	120	1.31	1.37	2926	3351
Morphology 8	3	480	1.33	1.31	3623	1775
Morphology 9	3	960	1.35	1.38	2178	4093

Table 2. Values of Coefficient (β) Fitting a Power Law to Each Simulated Morphology in the Drainage Volume Distribution

			Coefficient (β)		x_{min} (m^2)	
Simulation	Tidal Range (m)	D_{50} (μm)	Flood Tide	Ebb Tide	Flood Tide	Ebb Tide
Morphology 1	1	120	1.29	1.38	235,709.0	103,665.0
Morphology 2	1	480	1.37	1.37	191,368.6	208,435.4
Morphology 3	1	960	1.35	1.42	215,914.2	152,394.8
Morphology 4	2	120	1.32	1.37	371,395.1	641,016.2
Morphology 5	2	480	1.44	1.52	408,776.7	345,867.5
Morphology 6	2	960	1.40	1.44	737,292.7	993,107.7
Morphology 7	3	120	1.33	1.23	1398,016.1	963,937.9
Morphology 8	3	480	1.30	1.35	1511,610.0	877,350.7
Morphology 9	3	960	1.41	1.37	898,024.0	1012,457.5

3.4. Energy Expenditure

Rodriguez-Iturbe et al. [1992a] suggest that scale-invariant behavior in river networks and other natural systems may be a consequence of evolution toward least energy expenditure states, i.e., the appearance of fractal structures may be a requirement to reduce amount of energy dissipated by the system to the minimum. In this study, an evaluation of how energy expenditure changes as the morphology evolves toward equilibrium has been carried out. Figure 10 shows an exponential decay in the first years of morphological evolution. This occurs in a more pronounced way for increasing tidal range. The widening and deepening of the channels produces a reduction of the velocities, and as a consequence, also a reduction of the shear stress. The larger the tidal range, the longer it will take the system to reach equilibrium from the same starting configuration. This points out that larger tidal ranges in spite of having larger erosion capability (stronger currents), require a larger total work to achieve equilibrium because of the larger amount of sediment to be mobilized. The grain size also plays an important role in terms of energy dissipation, the smaller the grain size, the faster the system reaches equilibrium and so the minimum in energy expenditure. It should also be pointed out that larger tidal ranges converge to larger minimum energy expenditure values, i.e., the larger the tidal range, the larger the energy spent in the equilibrium state, due to larger system size and larger energy input per unit time.

3.5. Application to the Estuary of Santoña (Spain)

The methodology developed in section 2.2 was applied to the tidal network of Santoña (Figure 11a), which constitutes one of the most important salt marshes in the Cantabrian Coast (North of Spain) due to its biological productivity, as well as its role for wintering and as a passage for migratory birds. Tide is semidiurnal with a spring and mean tide of 5 and 3 m, respectively. Its tidal prism is 52.3 hm^3, around 70% of its surface (2000 ha) is intertidal and the fresh water input comes from the Ason River with an average annual flow of 16 m^3/s. The salt marsh vegetation covers around 834 ha (41.7% of the SantoñaÇs area).

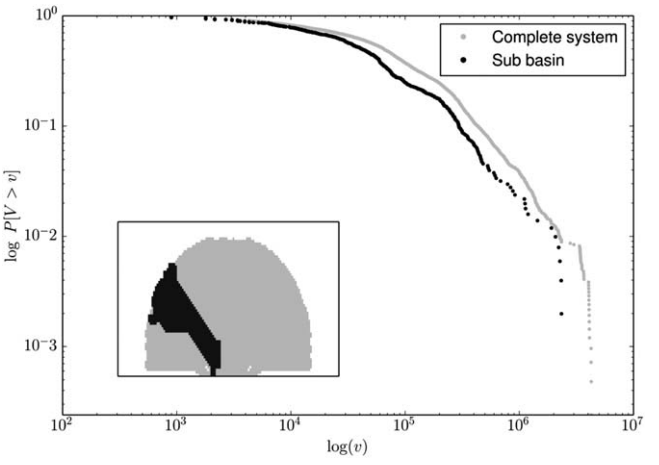

Figure 8. Exceedance probability of drainage volume at any point of the network computed for $D_{50} = 120$ μm and $TR = 1$ m during ebb time, over the whole basin (gray line), and in a cell selected in the outlet (black line). The drainage area of the subsystem is shown in the subplot with the darker colour.

A rectangular grid is used in the numerical computations covering an area of 10.35 × 15.35 km. A cell size of 50 m is used within the grid. A semidiurnal tide with a tidal range of 4 m has been used as forcing in the hydrodynamic model. The riverine input has not been taken into account due to its low relevance in the hydrodynamics of the system.

Figure 12 shows the distribution of volume drainage during an flood and ebb phase applying the

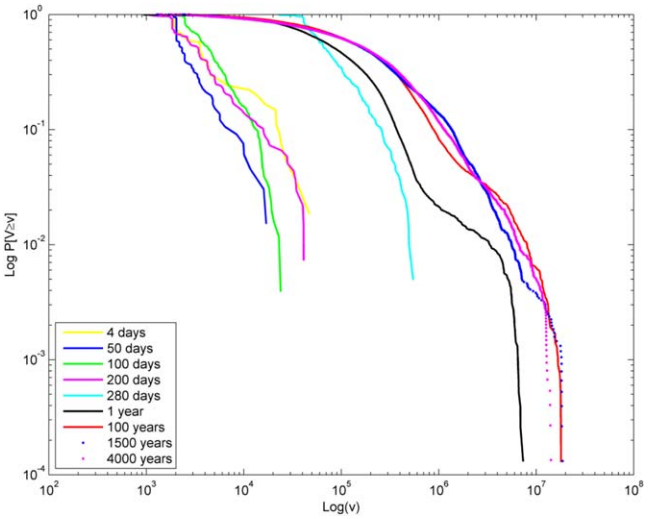

Figure 9. Exceedance probability of drainage volume at any point of the network computed along the time for $TR = 3$m and $D_{50} = 480$ μm and during ebbing time in: 4 days, 50 days, 100 days, 200 days, 1 year, 100 years, 1500 years, and 4000 years.

methodology developed in this work over the real bathymetry in the Santoña's estuary.

The distribution of the main channels shows similarities during both phases. It is in the secondary channels where most differences are observed. In order to obtain the volume drainage during a tidal phase in the whole basin, the connectivity between cells has to be transformed, removing loopy connections to finally obtain tree-like networks. During the process all cells belonging to a loop are detected, and the existing link between the first cell in the loop and the last cell involved is deleted. Also the water volume contained in the link removed is not accounted in the calculation of the total volume of water, which in turn induces a reduction in the total volume of the system, compared to the real one (in Santoña's case this reduction is around a 10% of the total volume). During the flood phase, the network drains a smaller amount of water than during the ebb phase, since during the flooding phase the flow tends

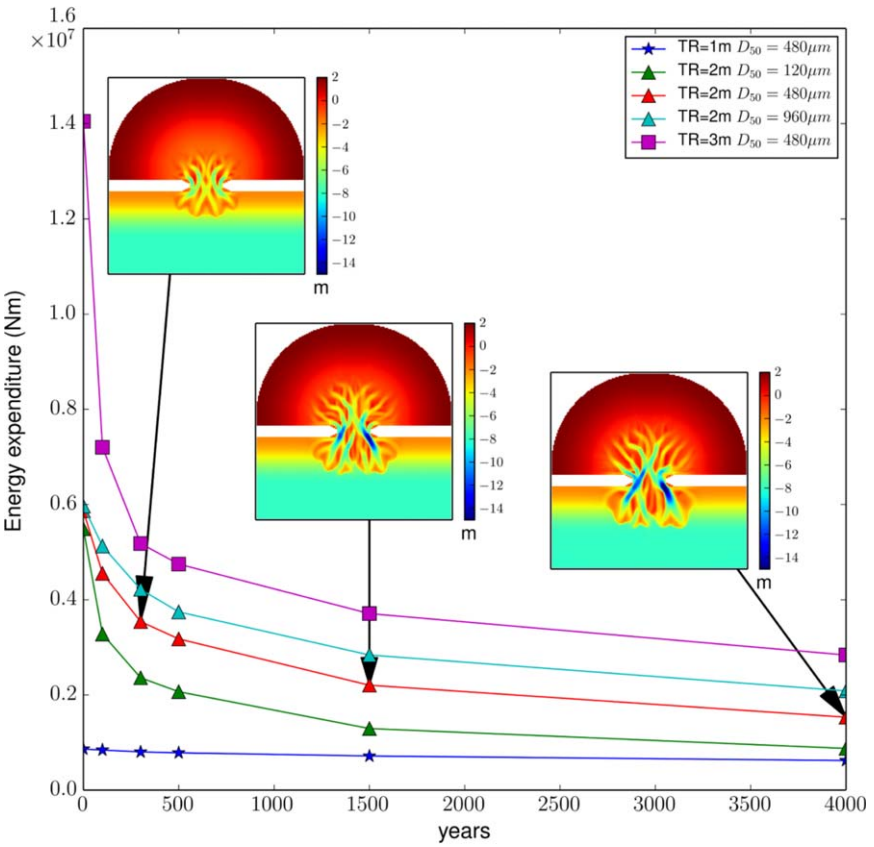

Figure 10. Energy expenditure over time (1, 100, 300, 500, 1500, and 4000 years) for the configurations with $TR = 1$ m and $D_{50} = 480$ μm, $TR = 2$ m, and $D_{50} = 120$, 480, 960 μm and $TR = 3$ m and $D_{50} = 480$ μm. The morphologies inside the figure correspond with the morphologies obtained with $TR = 2$ m and $D_{50} = 480$ μm during 300, 1500, and 4000 years.

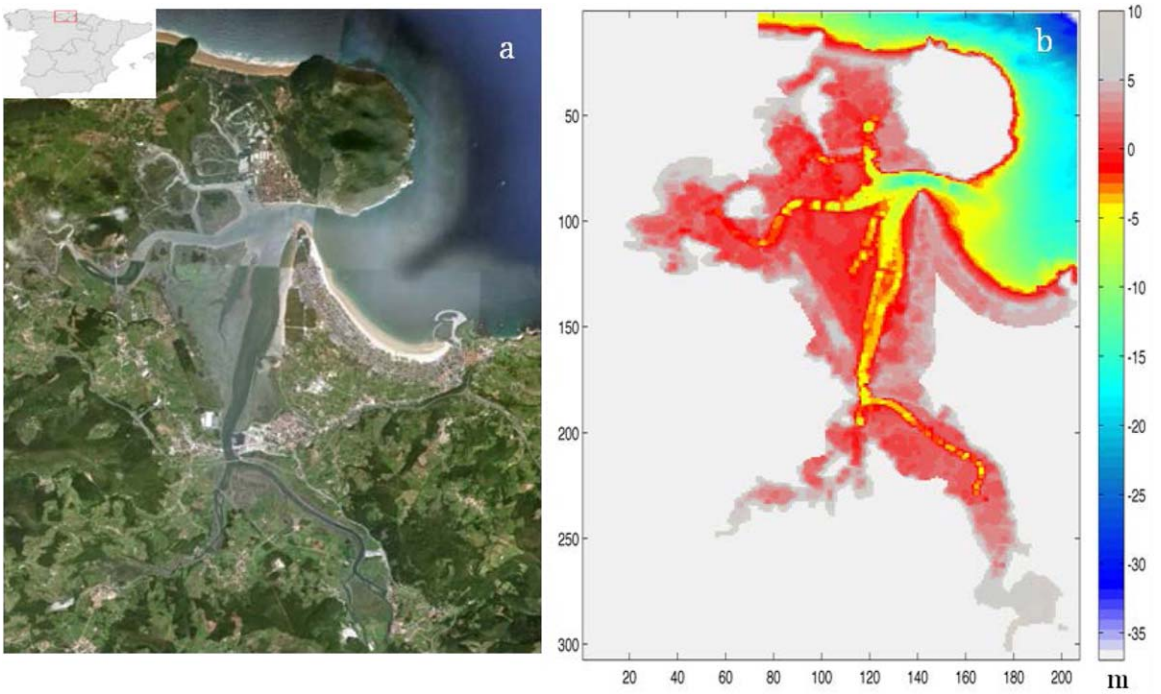

Figure 11. (a) Santoña's estuary and (b) bathymetry used in the hydrodynamic simulations (207 × 307 cells with a cell size of 50 m).

to contain more loops structures covering a larger portion of the domain. The probabilities of exceedance of drainage area and drainage volume have been computed. The exponents obtained from the power law fitting were 1.26 and 1.27, respectively (see Figure 13). These exponents are in the same range as the ones resulting from the numerical simulations of the idealized tidal basin (-1.39 ± 0.14 and 1.40 ± 0.13).

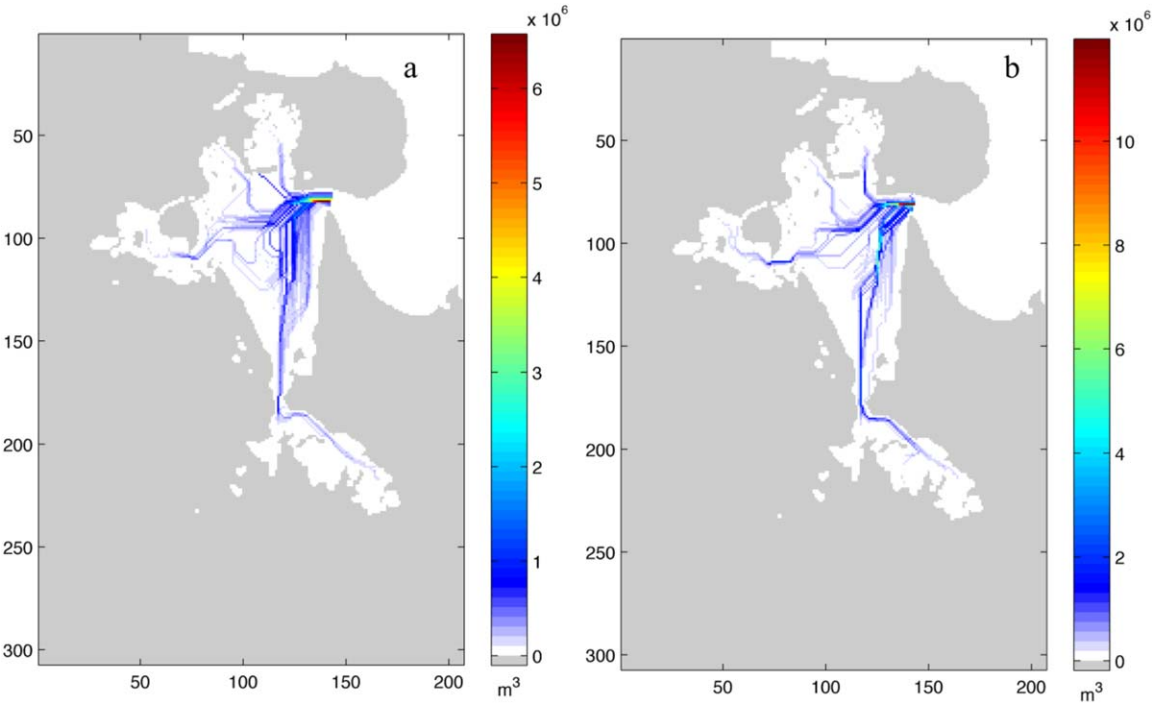

Figure 12. (a) Drainage volume in each grid cell during flooding phase and (b) drainage volume in each grid cell during ebbing phase.

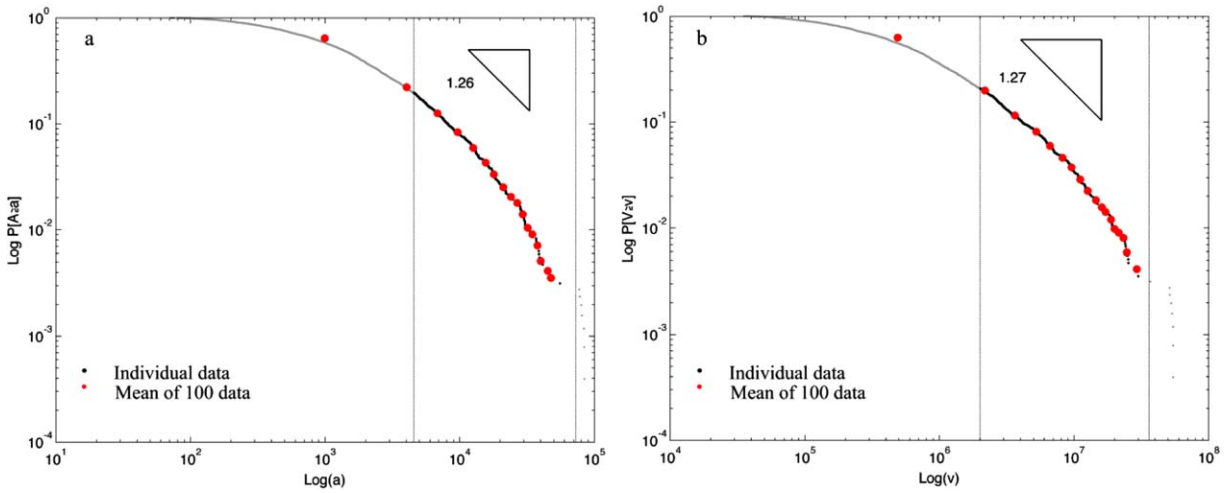

Figure 13. (a) Exceedance probability of drainage area P ($A \geq a$) at any point of the network (versus the current value of a expressed in m^2) computed in Santoña's estuary during ebb phase and (b) exceedance probability of drainage volume P ($V \geq v$) (versus the current value of v expressed in m^3) computed in Santoña's estuary during ebb phase.

An energy expenditure analysis has been performed in Santoña estuary considering its present configuration. The 2-D hydrodynamic model is applied, where bed friction is simulated by means of a uniform roughness coefficient, using a Manning's coefficient value of 0.02. A Manning's value of 0.02 is suitable in channels of sand [*Shaw et al*., 2010]. Similar values (0.026 $sm^{1/3}$) have been used in numerical studies [*Van Der Wegen et al*., 2008]. The energy expenditure value obtained was 3.5×10^6 N/m. As we have previously mentioned 41.7% of the area of Santoña is occupied by vegetation. It is for this reason that a new hydrodynamic simulation has been done, taking into account the friction produced by the vegetation with the objective to reproduce the real conditions. As presented in *Temmerman et al*. [2012] this is done by using a lower Manning n value of 0.02 in the nonvegetated areas (offshore and in the channels) and using a Manning with value 0.08 for the vegetated areas. The new conditions produce an increase of 33.2% in the energy expenditure of the system, showing the important role that vegetation plays in the flood attenuation as it has been shown in studies developed by *Costanza et al*. [2008] and *Wamsley et al*. [2010].

4. Discussion

Several authors [*Cleveringa and Oost*, 1999; *Angeles et al*., 2004; *Novakowski et al*., 2004] have analyzed the geometric and fractal characteristics of tidal networks using DEMs, satellite images and detailed maps by means of several techniques, Horton scaling laws, Hack's law and fractal dimensions, among others. However, all these studies are based on the analysis of the shapes and the geometric characteristics. These studies do not consider the hydrodynamic and morphodynamic characteristics of the system, limiting the possibility of a direct comparison with the aforementioned studies.

Future research should address the development of "benchmark" cases to specifically address differences with other techniques [*Cleveringa and Oost*, 1999; *Angeles et al*., 2004; *Novakowski et al*., 2004] and sensitivity of results.

A clear advantage of this methodology, in the case of estuaries at least, is that hydrodynamics and sedimentary processes are driven by the gradients of the free surface. Bed topography is a good proxy in the case of rivers, but it does not represent correctly flow dynamics in the case of estuaries.

The main disadvantage is that numerical simulations are required in order to define the drainage network. Methods base on bed topography provide solutions making only use of the DEM, but we require a simulation effort in order to study network connectivity.

Other studies have taken into account the flow dynamics using simplified approaches. For instance, *Rinaldo et al*. [1999a, 1999b] performed a detailed analysis of geometric and morphologic characteristics of a tidal basin using a simplified hydrodynamic model, in which the flow dynamics were represented by a Poisson

equation. This model, applied in different studies [*Marani et al*., 2003; *Feola et al*., 2005; *D'Alpaos et al*., 2007; *Di Silvio et al*., 2010], assumed that tidal propagation is dominated by friction. It also assumes tidal wave propagation is instantaneous through the channel network and thus the model is only suitable for shallow lagoons. *Rinaldo et al*. [1999b] concluded that there was a nearly complete lack of scale invariant. It should be remarked that our results are not directly comparable with the results presented by *Rinaldo et al*. [1999b]; not only the approaches to define the network are entirely different, but also the scales of the studies are different. The different nature of the systems under analysis (salt marshes in *Rinaldo et al*. [1999a, 1999b], sand-dominated estuaries in our case) combined with the different approaches used to define the network, make the two studies difficult to compare. Our analyses point out that the larger the tidal range, the larger amounts of channels are developed and the longer it takes to reach a slowly changing equilibrium configuration.

Our study involves a number of limitations. One of them is linked with the cell size used in simulations (100 m), which is coarse and which could pose a limit to the size of the minimum channel that can develop. Unlike *Rinaldo et al*. [1999a] and *Marani et al*. [2003] whose studies have been performed over much finer spatial scales, we have used a grid size of 100 m. This cell size is coarser, and limited the size of the minimum channel that could develop. A finer cell size would allow a finer-scale representation of the physical processes, although it has to be pointed out that these simulations would require a high-computational cost.

Due to the grid size used in this study, the value of x_{min} is limited and a direct comparison with the results of *Rinaldo et al*. [1999a, 1999b] and *Marani et al*. [2003], both characterized by channel widths $<$10 m and both indicating that there is not a single scaling regime, cannot be performed. An initial study on the role of grid size resolution is presented in *Jiménez et al*. [2014] and it indicates that down to grid size values of 50 m, the self-similarity is maintained. *Jiménez et al*. [2014] studied the impact of the grid size on the development of tidal network and its impact on the drainage area and the volume distribution. The authors show that the finer grid induces the formation of a greater number of narrower channels that dissect the tidal flats more uniformly increasing the drainage area. In terms of channel detection, solving the complete hydrodynamics equations leads to very complex flow solutions, where loop structures are present. As channel networks are derived from the hydrodynamics solution, loop structures must be eliminated in order to derive the proper drainage areas and drainage volumes in all the positions of the basin. Previous authors, studying tidal networks and using simplified hydrodynamics never dealt with loopy structures. Overall, the loop elimination process may induce some discrepancies in the total volume drained within the tidal basin.

Finally, as we have mentioned previously, power laws are signatures of scale-free, i.e., fractal behavior. However, power law fitting is a complicated procedure due to the nature of power laws; an additional large value may induce big changes in the estimated values for the exponent or the region over which the power law holds. The stability of the estimates depends on the amount and the specific characteristics of the data collected.

Our approach has allowed us to obtain the statistics of the drainage area, and also the statistics of the volume drained at every point of the tidal basin during a tidal cycle (ebb or flood). The volume drained is particularly important because it allows us to determine the regions where the flow is concentrated, i.e., the tidal channels. In this context, it worth noting that the drained volume is a controlling parameter in tidal basins and is normally used to define empirical equilibrium relations [*O'Brien*, 1931; *Walton and Adams*, 1976].

Analyzing our results for drainage area and drainage volume for different tidal ranges and sediment grain sizes we observe scale tendencies for both variables in 1–2 orders of magnitude. We have not considered other factors such as wind waves, overtides, cohesive material, and vegetation in order to reduce the number of physical processes in play and to simplify the source of variability in the results. We would like to point out that in the future the role of these factors will need to be considered, because of drainage conditions can potentially be altered and so the distribution function in the power laws.

Previous studies have focused on specific tidal basins, they have focused on specific tidal basin. Therefore, their conclusions and results may be biased to specific conditions of the tidal basin considered. In our study, however, different conditions of tidal range and sediment grain size have been analyzed for a simplified tidal basin, allowing us to derive more general conclusions and results. It is remarkable that the real estuary (Santoña estuary) has shown similar behavior to that observed in idealized example.

In the present work, the power law relationship is limited to 1–2 orders of magnitude, the narrow range of scale can be determine by the size of the system (delimit by the extension of the hydrodynamic field). Future studies should be focus on assessing the validity of the methodology over a larger range of scales.

Another analysis carried out in the present study is that of the tidal basin evolution toward a steady state from a far-from-equilibrium configuration. The evolution of energy dissipation over time as the tidal basin evolves was studied, to test if the same principle that drives river network evolution controls that of tidal basins. Our results indicate that tidal evolution is driven by the minimization of energy dissipation, which is in accordance with the results presented in *Van Der Wegen et al*. [2008] which show that tidal basins tend to less morphodynamic active states.

5. Conclusions

We have simulated the long-term morphological evolution of an idealized tidal basin for different tidal ranges and sediment grain sizes and also analyzed data from a real estuary. Applying the methodology presented in section 2.2 to the different morphologies, we can extract the following conclusions.

1. The drainage area and drainage volume distribution at any point in the tidal channels tend to follow the power law relationships $P[A > a] \propto a^{-1.39\pm0.14}$ and the $P[V > v] \propto v^{-1.40\pm0.13}$, respectively. These results are consistent for different tidal ranges and different grain sizes, as well as for the real estuary studied. While in the present work the power law relationship is limited to 1–2 orders of magnitude, future studies should focus on assessing the validity of the methodology and the results for systems characterized by a broader range of scales.

2. The same relationships are obtained for subbasins of the system, provided that the size of the subbasin is large enough to contain a network.

3. Over time the drainage area and the drainage volume distribution evolve toward a power law, when the minimum energy expenditure principle is fulfilled, i.e., initially the network does not exhibit any power law scaling, but as it gets closer to the equilibrium configuration, the system adjust to a power law scaling which is in turn related to the minimum energy expenditure. As in river systems the drainage configuration in tidal systems minimizes the total energy dissipation.

4. Nevertheless, our simulations only account for some of the important processes that shape tidal basins. A complete description introducing vegetation dynamics, overtides, cohesive sediment and wind, and riverine influence would be necessary in order to assess scale invariants in more general case.

This work presents a new step toward the understanding of the behavior of the tidal systems. In order to generalize our findings, our methodology should be tested for a large number of estuaries, presenting different morphologies and a variety of hydrodynamic characteristics.

References

Angeles, G. R., G. M. Perillo, M. C. Piccolo, and J. O. Pierini (2004), Fractal analysis of tidal channels in the bahía Blanca Estuary (Argentina), *Geomorphology*, *57*, 263–274.

Clauset, A., C. R. Shalizi, and M. E. J. Newman (2009), Power-law distributions in empirical data, *SIAM Rev.*, *51*(4), 661–703, doi:10.1137/070710111.

Cleveringa, J., and A. P. Oost (1999), The fractal geometry of tidal-channel systems in the Dutch Wadden Sea, *Geol. Mijnbouw*, *78*, 21–30.

Costanza, R., S. C. Farber, and J. Maxwell (1989), Valuation and management of wetland ecosystems, *Ecol. Econ.*, *1*, 335–361.

Costanza, R., O. Pérez-Maqueo, M. L. Martinez, P. Sutton, S. J. Anderson, and K. Mulder (2008), The value of coastal wetlands for hurricane protection, *Ambio*, *37*(4), 241–248.

D'Alpaos, A. (2005), Tidal network ontogeny: Channel initiation and early development, *J. Geophys. Res.*, *110*, F02001, doi:10.1029/2004JF000182.

D'Alpaos, A., S. Lanzoni, M. Marani, A. Bonometto, G. Cecconi, and A. Rinaldo (2007), Spontaneous tidal network formation within a constructed salt marsh: Observations and morphodynamic modelling, *Geomorphology*, *91*(3–4), 186–197, doi:10.1016/j.geomorph.2007.04.013.

Di Silvio, G., C. Dall'Angelo, D. Bonaldo, and G. Fasolato (2010), Long-term model of planimetric and bathymetric evolution of a tidal lagoon, *Cont. Shelf Res.*, *30*(8), 894–903, doi:10.1016/j.csr.2009.09.010.

Dissanayake, D. M. P. K., R. Ranasinghe, and J. A. Roelvink (2012), The morphological response of large tidal inlet/basin systems to relative sea level rise, *Clim. Change*, *113*(2), 253–276, doi:10.1007/s10584-012-0402-z.

Engelund, F., and E. Hansen (1972), A monograph on sediment transport in alluvial streams, Copenhagen: Teknisk forlag. p. 63.

Fagherazzi, S., and D. J. Furbish (2001), On the shape and widening of salt marsh creeks, *J. Geophys. Res.*, *106*(Cl), 991–1003.

Fagherazzi, S., A. Adami, S. Lanzoni, M. Marani, and A. Rinaldo (1999), Tidal networks: 1. Automatic network extraction and preliminary scaling features from digital terrain maps, *Water Resour. Res.*, *35*(12), 3891–3904.
Feola, A., E. Belluco, A. D'Alpaos, S. Lanzoni, M. Marani, and A. Rinaldo (2005), A geomorphic study of lagoonal landforms, *Water Resour. Res.*, *41*, W06019, doi:10.1029/2004WR003811.
Friedrichs, C. T., and D. G. Aubrey (1994), Tidal propagation in strongly convergent channels, *J. Geophys. Res.*, *99*(C2), 3321–3336, doi:10.1029/93JC03219.
Friedrichs, C. T., D. G. Aubrey, and P. E. Speer (1990), Impacts of relative sea-level rise on evolution of shallow estuaries, in *Coastal and Estuarine Studies*, edited by R. T. Cheng, vol. 38, pp. 105–120, Residual currents and long-term transport, Springer, N. Y.
Jiménez, M., S. Castanedo, Z. Zhou, G. Coco, R. Medina, and I. Rodriguez-Iturbe (2014), On the sensitivity of tidal network characterization to power law estimation, *Adv. Geosci.*, *1*, 1–5, doi:10.5194/adgeo-1-1-2014.
Katifori, E., and M. O. Magnasco (2012), Quantifying loopy network architectures, *PloS One*, *7*(6), e37994, doi:10.1371/journal.pone.0037994.
Lanzoni, S., and G. Seminara (1998), On tide propagation in convergent estuaries, *J. Geophys. Res.*, *103*(C13), 30,793–30,812, doi:10.1029/1998JC900015.
Lesser, G., J. Roelvink, J. Vankester, and G. Stelling (2004), Development and validation of a three-dimensional morphological model, *Coastal Eng.*, *51*(8–9), 883–915, doi:10.1016/j.coastaleng.2004.07.014.
Marani, M., E. Belluco, A. D'Alpaos, A. Defina, S. Lanzoni, and A. Rinaldo (2003), On the drainage density of tidal networks, *Water Resour. Res.*, *39*(2), 1040, doi:10.1029/2001WR001051.
Marciano, R., Z. B. Wang, A. Hibma, and H. J. de Vriend (2005), Modeling of channel patterns in short tidal basins, *J. Geophys. Res.*, *110*, F01001, doi:10.1029/2003JF000092.
Mileyko, Y., H. Edelsbrunner, C. A. Price, and J. S. Weitz (2012), Hierarchical ordering of reticular networks, *PloS One*, *7*(6), e36715, doi:10.1371/journal.pone.0036715.
Montgomery, D. R., and W. E. Dietrich (1988), © 1988 Nature Publishing Group, *Nature*, *336*, 232–234.
Morris, D. G., and R. G. Heerdegen (1988), Automatically derived catchment boundaries and channel networks and their hydrological applications, *Geomorphology*, *1*, 131–141.
Newman, M. E. J. (2005), Power laws, Pareto distributions and Zipf's law, *Contemporary Phys.*, *46*, 323–351.
Novakowski, K. I., R. Torres, L. R. Gardner, and G. Voulgaris (2004), Geomorphic analysis of tidal creek networks, *Water Resour. Res.*, *40*, W05401, doi:10.1029/2003WR002722.
O'Brien (1931), Estuary tidal prism related to entrance areas, *Civ. Eng.*, *1*, 738–739.
O'Callaghan, J. F., and D. M. Mark (1984), The extraction of drainage networks from digital elevation data, *Comput. Vision Graphics Image Process.*, *28*, 323–344.
Passalacqua, P., T. Do Trung, E. Foufoula-georgiou, G. Sapiro, and W. E. Dietrich (2010), A geometric framework for channel network extraction from lidar: Nonlinear diffusion and geodesic paths, *J. Geophys. Res.*, *115*, F01002, doi:10.1029/2009JF001254.
Rinaldo, A., S. Fagherazzi, S. Lanzoni, M. Marani, and W. E. Dietrich (1999a), Tidal networks 2. Watershed delineation and comparative network morphology, *Water Resour. Res.*, *35*(12), 3905–3917.
Rinaldo, A., S. Fagherazzi, S. Lanzoni, M. Marani, and W. E. Dietrich (1999b), Tidal networks 3. Landscape-forming discharges and studies in empirical geomorphic relationships, *Water Resour. Res.*, *35*(12), 3919–3929.
Rodriguez-Iturbe, I., and A. Rinaldo (1997), *Fractal River Basins: Chance and Self-Organization*, Cambridge University Press, Cambridge, U. K.
Rodriguez-Iturbe, I., A. Rinaldo, R. Rigon, R. L. Bras, E. Ijjasz-Vasquez, and A. Marani (1992a), Fractal structures as least energy patterns: The case of river networks, *Geophys. Res. Lett.*, *19*(9), 889–892.
Rodríguez-Iturbe, I., A. Rinaldo, R. Rigon, R. L. Bras, A. Marani, and E. Ijjasz-Vasquez (1992b), Energy dissipation, runoff production, and three-dimensional structure of river basin, *Water Resour. Res.*, *28*(4), 1089–1093.
Roelvink, J. A. (2006), Coastal morphodynamic evolution techniques, *Coastal Eng.*, *53*, 277–287, doi:10.1016/j.coastaleng.2005.10.015.
Shaw, E. M., K. J. Beven, N. A. Chappell, and R. Lamb (2010), *Hydrology in Practice* (fourth edition) CRC Press. 2, Park Square Milton Park Abindgon, OXON, OX1443N.
Stevens, P. (1974), *Patterns in Nature*, Little, Brown, Boston, Mass.
Tarboton, D. G. (1997), A new method for the determination of flow directions and upslope areas in grid digital elevations models, *Water Resour. Res.*, *33*(2), 309–319.
Tarboton, D. G., R. L. Bras, and I. Rodriguez-Iturbe (1991), On the extraction of channel networks from digital elevation data, *Hydrol. Processes*, *5*, 81–100, doi:10.1002/hyp.3360050107.
Temmerman, S., M. B. De Vries, and T. J. Bouma (2012), Coastal marsh die-off and reduced attenuation of coastal floods: A model analysis, *Global Planet. Change*, *92–93*, 267–274, doi:10.1016/j.gloplacha.2012.06.001.
Townend, I., and R. Dun (2000), A diagnostic tool to study long-term changes in estuary morphology, *Geol. Soc. Spec. Publ.*, *175*(1), 75–86, doi:10.1144/GSL.SP.2000.175.01.07.
Van der Wegen, M. (2013), Numerical modeling of the impact of sea level rise on tidal basin morphodynamics, *J. Geophys. Res.*, *118*, 1–14, doi:10.1002/jgrf.20034.
Van Der Wegen, M., Z. B. Wang, H. H. G. Savenije, and J. A. Roelvink (2008), Long-term morphodynamic evolution and energy dissipation in a coastal plain, tidal embayment, *Energy*, *113*, 1–22, doi:10.1029/2007JF000898.
Van Goor, M. A., T. J. Zitman, Z. B. Wang, and M. J. F. Stive (2003), Impact of sea-level rise on the morphological equilibrium state of tidal inlets, *Mar. Geol.*, *202*, 211–227.
van Maanen, B., G. Coco, and K. R. Bryan (2013a), Modelling the effects of tidal range and initial bathymetry on the morphological evolution of tidal embayments, *Geomorphology*, *191*, 23–34, doi:10.1016/j.geomorph.2013.02.023.
van Maanen, B., G. Coco, K. R. Bryan, and C. T. Friedrichs (2013b), Modeling the morphodynamic response of tidal embayments to sea-level rise, *Ocean Dyn.*, *63*, 1249–1263, doi:10.1007/s10236-013-0649-6.
Walton, T., and W. Adams (1976), Capacity of inlet outer bars to store sand, paper presented at the 15th Coastal Engineering Conference, pp. 1919–1937, Am. Soc. of Civ. Eng., Honululu, Hawaii.
Wamsley, T. V., M. A. Cialone, J. M. Smith, J. H. Atkinson, and J. D. Rosati (2010), The potential of wetlands in reducing storm surge, *Ocean Eng.*, *37*(1), 59–68, doi:10.1016/j.oceaneng.2009.07.018.
White, E. P., B. J. Enquist, and J. L. Green (2008), On estimating the exponent of power-law frequency distributions, *Ecology*, *89*(4), 905–912.
Zhou, Z., L. Stefanon, M. Olabarrieta, A. D'Alpaos, L. Carniello, and G. Coco (2014a), Analysis of the drainage density of experimental and modelled tidal networks, *Earth Surf. Dyn. Discuss.*, *2*, 105–116, doi:10.5194/esurf-2-105-2014.
Zhou, Z., M. Olabarrieta, L. Stefanon, A. D'Alpaos, L. Carniello, and G. Coco (2014b), A comparative study of physical and numerical modeling of tidal network ontogeny, *J. Geophys. Res.*, *119*, 892–912, doi:10.1002/2014JF003092.